Tensile force field takes crucial roles in local invasion of tumor cells through a mechano-chemical coupling mechanism

Jianfeng Meng,‡[abg] Xiangyu Xu,‡[bc] Chaohui Jiang,[ab] Peng Xia,[d] Pengfei Xu,[e] Liangfei Tian,[f] Yingke Xu,[f] Dechang Li,[a] Youhua Tan,*[g] Baohua Ji*[ah]

[a] Institute of Biomechanics and Applications, Department of Engineering Mechanics, Zhejiang University, Hangzhou 310027, China

[b] Wenzhou Institute, University of Chinese Academy of Sciences, Wenzhou 325001, China

[c] Key Laboratory of Biomechanics and Mechanobiology of Ministry of Education, Beijing Advanced Innovation Center for Biomedical Engineering, School of Biological Science and Medical Engineering, Beihang University, Beijing 100083, China;

[d] Zhejiang Provincial Key Laboratory for Cancer Molecular Cell Biology, Life science Institute, Zhejiang University, Hangzhou 310058, China

[e] School of Medicine, Zhejiang University, Hangzhou 310058, China

[f] MOE Key Laboratory of Biomedical Engineering, Zhejiang Provincial Key Laboratory of Cardio-Cerebral Vascular Detection Technology and Medicinal Effectiveness Appraisal, Department of Biomedical Engineering, Zhejiang University, Hangzhou, 310027, China

[g] Department of Biomedical Engineering, The HongKong Polytechnic University, Hong Kong, China

[h] Eye Center, The Second Affiliated Hospital, School of Medicine, Zhejiang University, Hangzhou, 310027, China

* Corresponding authors: Youhua TAN (youhua.tan@polyu.edu.hk), Baohua JI (bhji@zju.edu.cn)

‡ These authors contributed equally to this work.

Abstract

Cancer metastasis starts from early local invasion, during which tumor cells detach from the primary tumor, penetrate the extracellular matrix (ECM), and then invade neighboring tissues. However, the cellular mechanics in the detaching and penetrating processes have not been fully understood, and the underlying mechanisms that influence cell polarization and migration in the 3D matrix during tumor invasion remain largely unknown. In this study, we employed a dual tumor-spheroids model to investigate the cellular mechanisms of the tumor invasion. Our results revealed that the tensional force field developed by the active contraction of cells and tissue plays pivotal roles in tumor invasion, acting as the driving force for remodeling the collagen fibers during the invasion process. The remodeled collagen fibers promoted cell polarization and migration because of stiffening of the fiber matrix. The aligned fibers facilitated tumor cell invasion and directed migration from one spheroid to the other. Inhibiting/shielding the cellular contractility abolished matrix remodeling and re-alignment and significantly decreased tumor cell invasion. By developing a coarse-grained cell model that considers the mutual interaction between cells and fibers, we predicted the tensional force field in the fiber network and the associated cell polarization and cell-matrix interaction during cell invasion, which revealed a mechano-chemical coupling mechanism at cellular level of the tumor invasion process. Our study highlights the roles of cellular mechanics at the early stage of tumor metastasis, and may provide new therapeutic strategies for cancer therapy.

Keywords: tumor invasion, cell migration, cell polarization, matrix remodeling, coarse-grained model, numerical simulation

1. Introduction

Metastases account for the great majority of cancer-associated deaths, yet this complex process remains one of the most challenging aspects in cancer biology.[1, 2] It is a general consensus that local invasion is the initial step of metastasis.[1] Therefore, prohibiting the occurrence of early

invasion would resist metastasis and thus increase patient survival.[1] It was shown that the development of tumor invasion is related to not only the intrinsic changes in tumor cells but also the properties of the tumor microenvironment.[3, 4] For instance, the physical properties of ECM undergo significant changes before/during the invasion, such as increased stiffness[5-7] and structural alterations[8-10] due to the remodeling of ECM by the cell and tissue.[11-13] The mechanical signals induced by the change of ECM would then be detected by tumor cells and translated into stimuli through intracellular signaling pathways that would induce malignant phenotypes.[14-16] In contrast, reducing matrix stiffness and remodeling degrees can suppress the invasiveness of tumor cells.[8, 17] Therefore, it is reasonable to speculate that the structural and mechanical properties of the tumor microenvironment are closely related to the local invasion. However, the cellular mechanics of the mechanical microenvironment influencing tumor progression remains largely unknown.

Recently, there has been a surge of interest in investigating the role of physical properties of microenvironment in tumor cell invasion. For instance, it was found that when seeded in a stiff hydrogel mimicking the mechanical environment of breast carcinoma in vivo, MCF10A cells developed into a cancer organoid with invasive branches; in contrast, cells inoculated in a soft matrix grew into a normal acinar structure.[18] Moreover, the microstructure of ECM would also play important roles. For instance, Koorman et al. observed an enhanced alignment of collagen fibers around invasive tumors, and an increased number and length of tumors' invasive strands with thick collagen fibers.[19] And Wang et al. found that the aligned fibers increased the migration speed of both collective multicellular chains and single cells compared with the fiber networks with random or orthogonal configurations.[16] Furthermore, Han et al. showed that the oriented fibers promoted the invading process of metastatic cells. They therefore proposed a "tissue treatment" therapy that considers changing the orientation of the ECM fiber structure to minimize the invasion rate of metastatic cells.[20] However, it is not quantitatively understood why and how the alignment of matrix fiber influences cell polarization and then their detaching and

migration from the primary tumor.

To explore the underlying mechanisms of tumor invasion, numerical simulations have been extensively adopted to study the quantitative mechanisms that regulate the invasion process. These numerical approaches can overcome the limitations in the experiments restricted by current techniques with respect to the spatial and temporal resolution considering the complexity of the tumor-matrix system. For instance, Ahmadzadeh et al. developed a chemomechanical model to investigate how melanoma cells invade the collagen matrix, and how the alignment and stiffness of collagen fibers influence the invasion.[21] Pal et al. used the Cellular Potts Model to investigate how tumor cells interact with different types of matrix fibers. They found that the ECM fibers with aligned structures provided contact guidance that increases the invasiveness of cancer, while there was minimal local intravasation in randomly curved ECM fibers.[22] Moreover, by employing a two-dimensional cellular model, Li et al. found that the reduced cell-cell adhesion between tumor cells or increased cell-ECM adhesion would lead to the development of a more invasive tumor phenotype.[23] However, the existing models still cannot provide a quantitative understanding of the cellular process of tumor invasion; for instance, how active contraction of cells and tissue influences the evolution of the stress field in the matrix and then the cell polarization and migration is unknown.

In this study, we developed a dual tumor-spheroid system for studying the mechanisms of local invasion through experiments with in situ observation of tumor invasion and numerical simulation with quantitative analyses. We analyzed the effects of physical factors such as tumor spheroid size, tumor spheroid distance, cellular contraction, and collagen fiber density on tumor invasion. We found that the tumor spheroids' contraction effectively remodeled the collagen fibers around the tumor spheroids, which enhances the polarization of tumor cells around the peripheral of tumor spheroids. We showed that the tension in tumor spheroids and matrix is crucial for the alignment and stiffening of matrix/collagen fibers. This tensional field is necessary for cell polarization and stiffening of the matrix by enhancing the cell-matrix

interaction, which promotes the invasive migration of tumor cells. The realignment and stiffening of ECM fibers further stimulated tumor cells to invade the matrix with higher migration velocity and persistence. In contrast, inhibiting/shielding cell contraction wiped out collagen fiber remodeling, thereby weakening tumor invasion. Interestingly, the density of collagen fibers exhibited a biphasic effect on tumor cell invasion. Compared to an intermediate density of collagen fiber matrix, either a decrease or increase in fiber density resulted in a reduction in both the number and velocity of invading tumor cells.

2. Materials and methods

2.1 Cell culture

The mouse breast cancer cell line 4T1 was purchased from American Type Culture Collection (ATCC). The cells were cultured in DMEM with 10% fetal bovine serum (Gibco, USA) and 1% penicillin/streptomycin (Gibco, USA) under the condition of 37 °C and 5% CO_2. The cells were passaged every two days to maintain their viability.

2.2 Construction of dual tumor-spheroids model

The tumor spheroids were produced using the classical hanging drop method (Figure 1).[24] Firstly, cells with a confluency of approximately 70% were detached using 0.25% trypsin with EDTA (Thermo Fisher Scientific) in a T25 flask (Corning, USA). The same volume of medium was then added to neutralize the trypsin solution. After centrifugation at 1000 rpm for 5 minutes, the cell pellets were resuspended in 5 ml of medium containing 0.12% methylcellulose (Sigma Aldrich, USA), and approximately 10 μl of the sample was counted. To obtain the tumor spheroid of varied sizes, we controlled the cell number in the 10 μl droplet. For example, the solution containing 300, 500, 800, and 1500 cells can form a tumor spheroid of 100, 200, 300, and 400 μm in diameter, respectively.

To create the Type I collagen solution, we used a mixture of 10% 10×DMEM medium

(Gibco, USA), 1% insulin (Sigma Aldrich, USA), PBS buffer (Gibco, USA), and rat tail Type I collagen (Corning, USA). The collagen solution was neutralized to pH 7.4 using 0.1M NaOH. We adjusted the Type I collagen ratio and the PBS buffer volume to achieve the desired collagen concentration. To visualize the collagen fibers, a suitable amount of FITC-labeled Type I collagen (Sigma Aldrich, USA) was added to the collagen solution, and the mass ratio of labeled collagen to unlabeled collagen was maintained at 1:20.

Initially, the 10 μl cell suspension droplets were deposited on the lid of a culture dish, as illustrated in Fig. 1A. There were approximately 20 droplets that were hung from the lid of a 60 mm culture dish containing approximately 2 ml of PBS buffer to prevent droplet evaporation. The droplets were left to incubate in the culture chamber for about 2 days to form tight spheroids (Fig. 1A).

Once the tightly compacted tumor spheroids were obtained, the culture medium surrounding the spheroids was removed from the hanging droplets, and they were resuspended simultaneously with 10 μl of collagen solution, which were then injected into a confocal dish with a polymerized collagen layer at the bottom (Fig. 1B). The sample was polymerized at 21°C for 30 minutes, and then a warm culture medium was slowly added. The samples were examined under a microscope, and the distance between dual-tumor spheroids was measured using imaging software. By restricting the number of spheroids in the 10 μl of collagen solution, the distance between the spheroids can be controlled, e.g., 3-4, 5-6, and 7-8 tumor spheroids can generate dual-tumor spheroids with the distance of 240, 180, and 120 μm, respectively.

After obtaining suitable dual-tumor spheroids, an appropriate amount of collagen solution was added to submerge the spheroids completely. Then, the sample was transferred to a live-cell workstation for time-lapse microscopy (Fig. 1C). To investigate the cellular mechanics of the local invasion of tumor cells, we focused primarily on the region between two adjacent tumor spheroids (see inset in Fig. 1C).

2.3 Cell staining and live-cell imaging

The tumor spheroids were pretreated with Sir-actin Kit (Cat# CY-SC001, Cytoskeleton, Inc.) at a dilution of 1:1000 for 12 hours, along with Hoechst 33342 (Cat# H1399, Invitrogen) at a concentration of 10 μg/ml for 30 minutes, before being seeded onto a FITC-collagen gel. To minimize photobleaching, a Carl Zeiss T-PMT confocal microscope equipped with a Pln Apo 20×/NA 0.8 objective was used to capture images using lasers with wavelengths of 405, 488, and 647 nm. The time-lapse setting was 8 hours with an interval of 15 minutes, generating 12 optical slices with a thickness of approximately 20 μm. All images were processed and analyzed using ZEISS ZEN 3.7 software. The live-cell experiments were conducted at 37 °C and 5% CO_2. For inhibition experiments, the samples were preincubated with specific drug concentrations for 1 hour and maintained throughout the experiment.

2.4 Multiphoton laser ablation

Laser ablation of collagen fibers was performed by the pulsed laser with 800 nm wavelength based on Mai Tai HP Ti: Sapphire compact laser system. The ablated region was defined by a 512 × 64 pixels rectangular area for the 20× objective at a given distance away from the tumor-spheroid edge, and the ablated space was created by the scanning of 60 μm thick Z-stacks with 50 optical sections. To make sure that collagen fibers were thoroughly ablated, the pulsed laser with 60% intensity was utilized to scan the ablated space at least three times. After the laser ablation, the process of tumor invasion would be imaged under the microscope.

2.5 Analysis of cells geometry and migration

The contour of the tumor cell was obtained by using ImageJ software, which was then fitted to an ellipse using the least squares fitting method. Then, the coordinates of the center of the ellipse, the semi-major and semi-minor axis, and the angle between the major axis and the x-axis were obtained. The cell aspect ratio was calculated as the ratio of the semi-major to the semi-minor axes of the ellipse. To track the movement of invading cells, we used the Manual Tracking plugin in ImageJ, recording the coordinate information of each cell at regular time intervals.

Remarkably, we only analyzed the cells that remained in the view throughout the entire experiment, excluding any dividing or non-motile cells. Using the recorded cell coordinates, we plotted the migration trajectories and calculated cell velocities.

To evaluate the persistence of cell migration, we introduce the directional persistence index (DPI), defined as the ratio of the displacement to the total path length of cell trajectory.[25] If a cell migrates randomly, the value of DPI is low, which means the directionality of cell migration is low. If the directionality of cell migration is high, then the value of DPI is high. To ensure statistical rigor, all experiments were conducted in triplicate, and more than 100 cells were evaluated for each replicate.

2.6 Analysis of collagen fiber network

We employed a Carl Zeiss T-PMT confocal microscope equipped with a Pln Apo 40×/NA 0.95 objective to visualize FITC-collagen gel, and characterized the structure of the collagen fiber network using 488 nm excitation light. Approximately 20 μm thick Z-stacks were obtained by collecting 12 optical sections, which were then maximumly projected to one image for structural analysis using CurveAlign software and ImageJ.[26, 27] The CT-FIRE module of CurveAlign software was utilized to evaluate individual collagen fiber properties, such as length, width, and straightness. Furthermore, we analyzed the alignment of the entire collagen gel structure using the CFR-mode without boundaries. All analyses were performed with the default settings of CurveAlign software. Collagen density was measured using ImageJ, and parameters were kept consistent during the analysis. To compare the differences in collagen gel structure between invasion and non-invasion sites, at least 3 image areas of 30 × 30 μm were selected around each site, and the mean values were treated as a data point.

The alignment coefficient of fibers was analyzed using CurveAlign 4.0 software. Briefly, CT-FIRE module in CurveAlign 4.0 software was applied to extract the endpoints of collagen fibers for the fluorescence image and save the fiber endpoints in a database file. A feature vector $p_k \in X$ was then built for each fiber using its two endpoints in the image. The fiber alignment

coefficient was calculated based on the following formula:

$$\sigma = \frac{1}{N}\left|\sum_{X} \exp\left(i \times 2\theta_k\right)\right|$$

where $\theta_k \in \{0, \ldots, \pi\}$ is the angle of p_k in X with respect to the horizontal direction, and N is the total number of fibers in the image. Therefore, the alignment coefficient is calculated as the normalized vector sum of the directional vectors. The larger the vector sum, the higher the degree of the fiber alignment.[9]

2.7 Measurement of collagen fiber displacement

The displacement of collagen fibers was measured using MatPIV1.6.1 program developed by J.K. Sveen from the University of Cambridge.[28] Two consecutive image Z-stacks of collagen fibers were acquired with a 15-minute time interval, and each image stack was projected onto a single image. The mask.m module was utilized to exclude the tumor area from the image, and the displacement between the sequential images was computed. Subsequently, both images were divided into smaller regions, which are known as sub-windows. Each sub-window in the first image was compared with the corresponding sub-window in the second image to obtain the displacement of collagen fiber. To calculate the displacement, a time interval of 15 minutes and a 50% overlap region were set. The window shifting technique was employed to process the images iteratively. The displacement vectors resulting from the difference images were filtered, and the missing vectors were interpolated using the nearest neighbor method.

2.8 Statistics and reproducibility

All graphs and statistical analyses were conducted using GraphPad Prism 8 software. Data are presented as mean ± standard error of the mean (SEM). Differences between invasive and non-invasive sites were evaluated using one-sample t-tests. Differences in collagen structure and invasive cell behavior under various conditions were detected using the one-way analysis of variance (ANOVA). Statistical significance was set at $P < 0.05$, and all significant differences are

indicated in the corresponding figures with an asterisk (*). Unless otherwise stated, all results were reproducible in at least three independent experiments. Note that all the analyses were conducted within the region of interest (ROI) depicted in Figure 1C. And the dimension of the ROI was always kept fixed.

2.9 Numerical modeling methods

Here we developed a coarse-grained (CG) model for simulating the invasion behaviors of tumor cells (See Fig. S1). This model is an extension of our previous models for simulating multiple cell behaviors.[29, 30] In the model, we use the CG particles to represent the membrane and cytoskeleton of the cell, of which the interaction between CG particles was modeled by bonded or nonbonded interaction (Fig. S1B). We further introduced prestrain in the bond interaction in cytoskeleton to consider the active contraction of cell. The cell would be deformed under its active contraction and external forces from neighboring cells. Figure S1D highlights the intracellular and intercellular forces considered in a multi-cellular model system.

In addition, in this new CG model we introduced the cell-fiber matrix interaction. The ECM fibers were also discretized by using CG particles that are connected by bonded interactions. Between/among the fibers the bonded interaction was used to model the crosslinking for the formation of a fiber network (Fig. S1E). Fiber density was adjustable and the orientation of the fibers in the network was randomly arranged. The adhesion force, called cell traction force, between cells and ECM fibers, is modeled by Lennard-Jones potential between particles of the cell and those of fibers within a distance threshold. It was shown that the imbalance of cell traction force during detachment of the cell rear generates the driving force for cell migration (see more details in Supplementary Materials).[31, 32]

3. Results

3.1 Cellular mechanics of tumor invasion under contraction of tumor spheroids

To investigate the cellular mechanisms underlying the detachment of tumor cells from primary tumor, we adopted a dual tumor-spheroid system (Fig. 1). After the tumor spheroids were seeded into the fiber matrix, there is a strong interaction developed between the tumor spheroids and the collagen matrix, particular at the region between the two tumor spheroids. The contraction of the tumor spheroids severely remodeled the collagen matrix network by re-aligning the collagen fibers, which paved a way for tumor cell invasion. In the following analyses, the statistics were all conducted within ROI depicted in Fig. 1C.

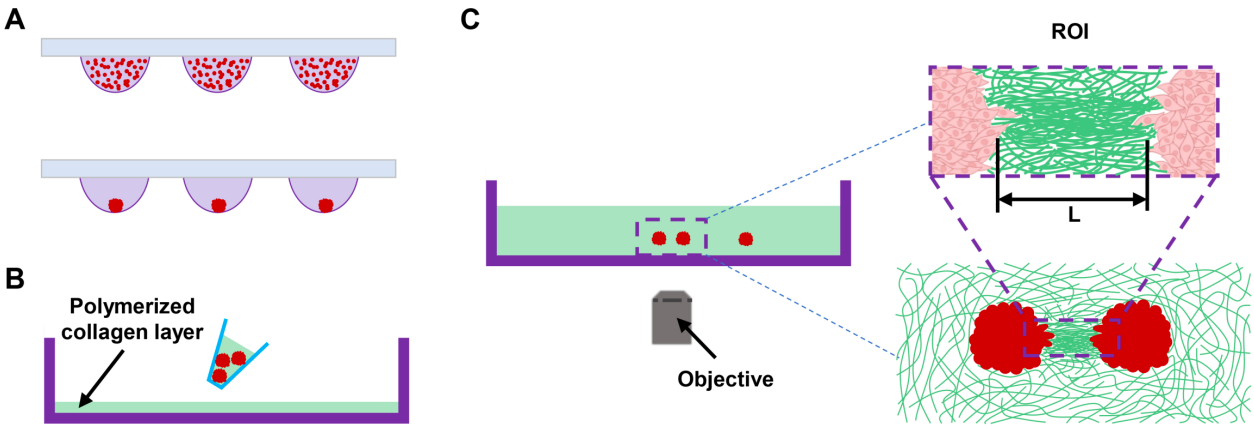

Fig. 1 Schematic of the method and process of embedding dual tumor-spheroids into the collagen gel matrix. (A) The 10 µl cell suspension droplets were suspended on the lid of a culture dish (upper). Dense spheroids were formed after 2 days in the suspended droplet (bottom). (B) The tumor spheroids were resuspended in the 10 µl of collagen protein solution, and then seeded onto the collagen protein layer in the culture dish. (C) An appropriate amount of collagen protein solution was added to submerge the tumor spheroids completely, and the tumor invasion process is ready for time-lapse imaging. The inset shows the region between the tumor spheroids as the region of interest (ROI), where 'L' indicates the distance between the inner edges of the two tumor spheroids.

Figure 2A illustrates the fluorescence image of the remodeled collagen fiber network and the detached tumor cells migrating along the collagen fibers for a distance of 120 µm between the two tumors. Correspondingly, the trajectory of the detached tumor cell was given on the right, showing it migrated from one tumor spheroid to the other. Figures 2B-D show how the distance

between the two tumor spheroids affects the remodeling of the collagen fiber network and the trajectories of invading tumor cells when the distance was increased to 180 μm, 240 μm and infinite (i.e., one tumor spheroid). When two tumor spheroids were infinitely far apart, they would hardly have any influence on each other. In this case, the invasion behavior of the two tumor spheroids should be similar to that of a single one. And the trajectory of the detached tumor cells became less directional with the increase of the distance.

For a quantitative evaluation of the directionality of cell migration, we calculated the DPI of the trajectory of the invading tumor cells (Fig. 2E), which progressively decreased along with the increase of the distance between the two spheroids (Fig. 2E). These results suggest that the persistence of migration of tumor cells from one spheroid to the other depends on the separation distance. In addition, the velocity of invading cells gradually increased over time and decreased over distance (Fig. 2F). Correspondingly, Fig. 2G shows that a larger distance between tumor spheroids resulted in less invading tumor cells. Note that the increasing velocity of tumor cells is due to the increased fiber alignment under the contraction of the spheroid, which highly promoted the directionality of cell migration.

To understand the mechanisms of this distance-dependent cell invasion, we analyzed the characteristics of the evolving collagen fiber network between the two spheroids. Our results showed that the fiber alignment coefficient progressively decreased when the distance between the two spheroids increased (Fig. 2H), suggesting that the remodeling of collagen fibers by tumor spheroids produced a highway for tumor cells for their invading process. The shorter the distance between the spheroids, the higher the degree of the remodeling of the fiber network by the contraction of the spheroids. In addition, we compared the alignment coefficient of fibers between invasive and non-invasive sites (see Fig. S2E-G), confirming the close relationship between tumor cell invasion and the external microenvironment.

Furthermore, we analyzed the relationship between cell polarization and fiber alignment. We used θ to represent the angle between the direction of cell polarization and the line

connecting the center of the two tumor spheroids, showing that the cells tend to polarize and invade more along this line when the distance between tumor spheroids was smaller (Fig. 2J). This result was consistent with the trend of collagen fiber alignment (Fig. 2H).

Moreover, we found that the polarity of the invading tumor cells gradually increased over time during the invading process along with the reduction of the separation distance between the tumor spheroids (Fig. 2I). The high polarity of tumor cells was reminiscent of the mesenchymal phenotype. This could be attributed to the elevation in the transient stiffness of the realigned matrix under the increased deformation of the fiber matrix, as the collagen fiber is a typical hyperelastic material. The increased stiffness of the fiber matrix might further promote cell polarization and migration.

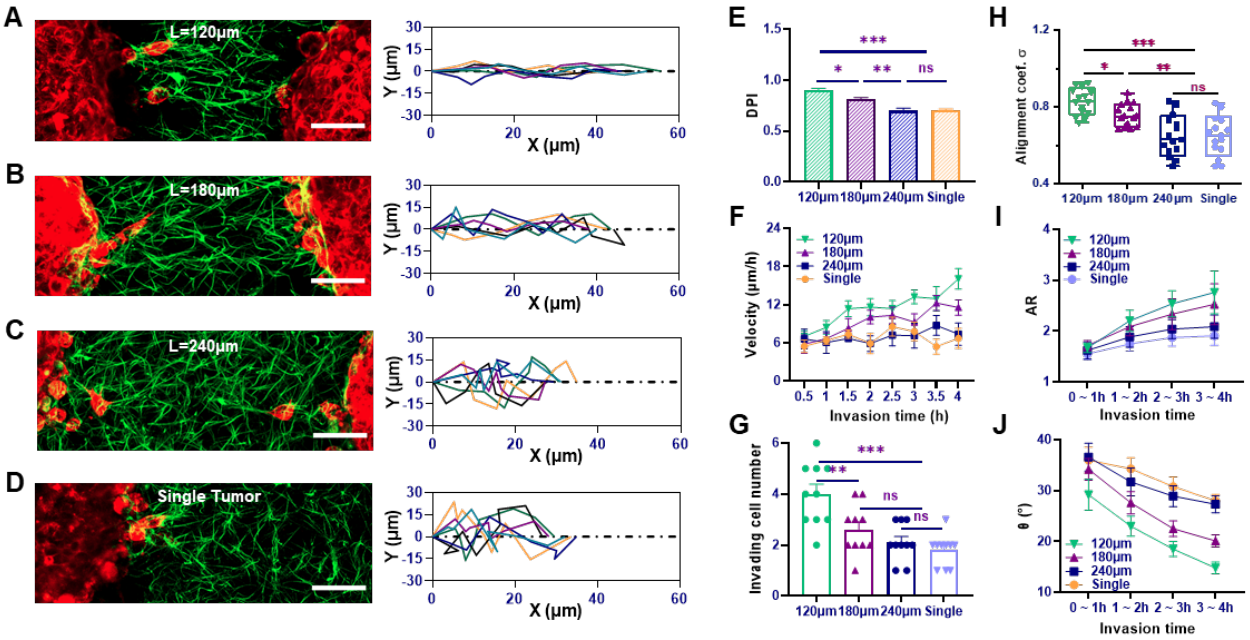

Fig. 2 Effect of the distance between the two tumor spheroids on tumor cell invasion. (A-C) Fluorescence images of tumor cells detaching and invading the collagen fiber matrix for various distances between the two tumor spheroids of 120 μm, 180 μm, 240 μm, respectively. On the right are the corresponding cell trajectories of the invasion process. (D) Fluorescence image of tumor cell and matrix and corresponding cell trajectory of a single tumor spheroid mimicking the case of infinite distance between two tumor spheroids. Red represents cells, and green represents collagen fibers, with a scale bar of 50 μm. (E) The directional persistence index (DPI) of invading tumor cells. (F) The evolution of the velocity of invading tumor cells as a function of the

invasion time. (G) Number of detaching and invading tumor cells from the tumor spheroids per 100 μm of arc length of the tumor spheroid. (H) Alignment coefficient of collagen fibers in the region between the tumor spheroids. (I) The evolution of the aspect ratio of invading tumor cells as a function of invasion time. (J) The evolution of angle θ as a function of the invasion time. The statistical analysis of the significance of the difference in panels E, G, and H was conducted using the one-way ANOVA method.

3.2 Fiber density exhibits biphasic effect on tumor invasion

We have shown that the spheroid distance influenced the tumor invasion through affecting the remodeling of the fiber matrix. It is expected that the fiber density should also play essential roles in the behaviors of tumor invasion. To explore its effect, we altered the concentration of collagen solution from 0.5, 1, to 2 mg/ml during the preparation of the fiber matrix. Figure 3A shows the fluorescent images of tumor invasion at three different concentrations. Our measurement showed that fiber density increased along with collagen concentration, while the diameter of the fibers remained relatively unchanged (Fig. 3B, C). The increase of the fiber density might raise the stiffness of collagen fiber network, making it difficult to deform under the contractility of the tumor. Indeed, the fiber alignment coefficient decreased with the increase of the fiber density for spheroid distance of 180 μm (Fig. 3D), which could reduce cell invasion. On the other hand, cell-fiber adhesion would be strengthened with the increase of the fiber density, which had the potential to promote tumor cell invasion. As a result, there is a biphasic effect of fiber density on the number of invading cells (Fig. 3E). Same phenomena were also observed in the invasion of single tumor spheroid (Fig. S3).

Furthermore, fiber density exhibited similar biphasic effect on cell migration velocity while having slight influence on cell polarity (Fig. 3F and 3G). That is, the tumor cells exhibited the highest invasion velocity at the 1 mg/ml collagen density (see Fig. 3G). This outcome might be attributed to the fact that the fiber matrix with collagen density of 1 mg/ml was effectively remodeled by the tumor spheroids, and at the same time could provide the most effective cell-fiber adhesion for tumor cell migration. This kind of biphasic effect of fiber density on cell migration was similar to the effect of the quantity of cytoskeleton for force transmission from

outside of the cell to the nucleus.[33]

In addition, fiber density could further influence the migrating direction (cell angle θ) of tumor cells. The cell angle increased along with the fiber density, suggesting that the increase of deviation of the migrating direction from the center-center line between the two tumor spheroids (Fig. 3H). This was further supported by the reduction of the DPI (Fig. 3I), which might be explained by the fact that the increase of fiber density enhances the fiber stiffness and the difficulty to remodel the fiber network. Similar findings were also observed when the distance between two spheroids was increased to 240 μm (Fig. S4).

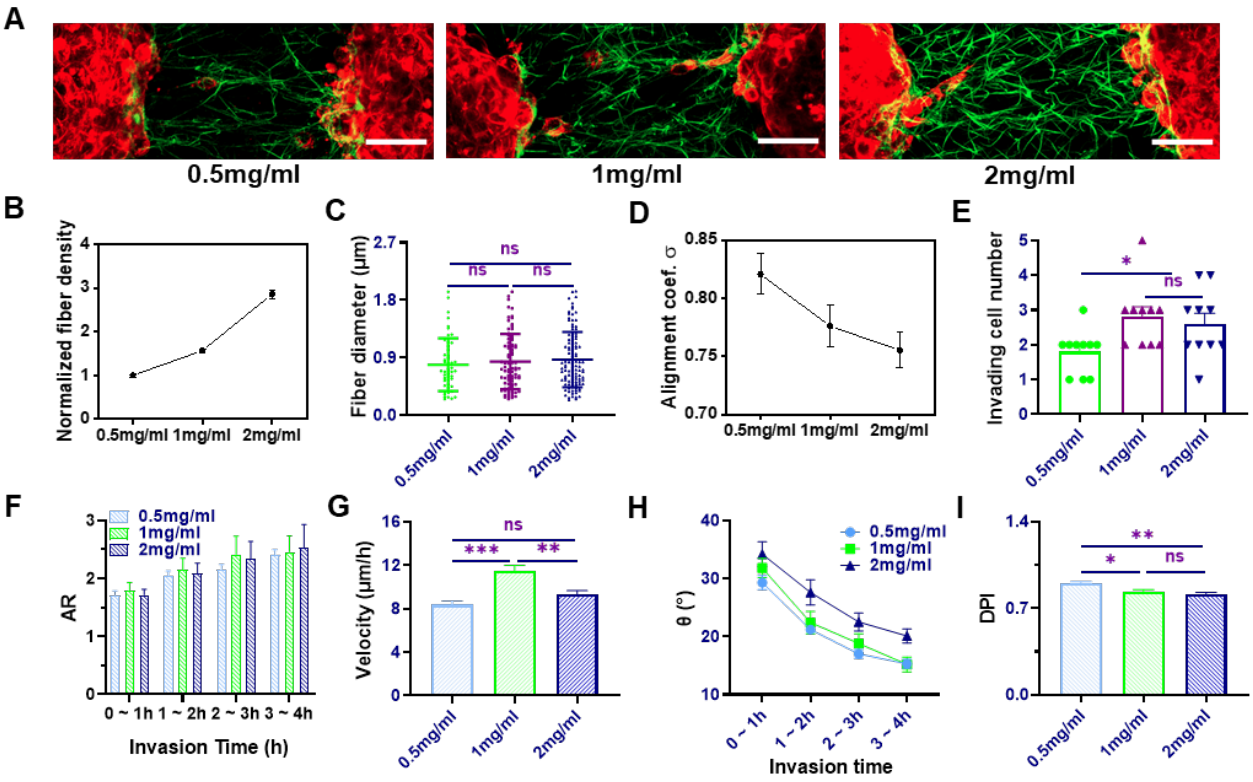

Fig. 3 Effect of fiber density on the tumor invasion. (A) Fluorescence images of tumor invasion in fiber matrix with three different collagen concentrations of 0.5, 1, and 2 mg/ml. Red represents cells, and green represents collagen fibers. The scale bar is 50 μm. The spheroids distance L= 180 μm. (B) Normalized collagen fiber density as a function of collagen concentrations. (C) Fiber diameter for three different collagen concentrations. (D) Alignment coefficient of collagen fibers as a function of collagen concentrations. (E) Number of invading tumor cells per 100 μm arc length of tumor spheroids for different collagen concentrations. (F) The aspect ratio of invading tumor cells as a function of invasion time. (G) The average velocity of invading tumor cells for three different collagen concentrations. (H) The angle θ as a function of invasion time.

(I) The DPI of invading tumor cells for different collagen concentrations. The statistical analysis of panels E, G, J, and K was conducted using the one-way ANOVA method.

3.3 Tumor spheroid size promotes matrix remodeling and tumor cell invasion

We found that the size of tumor spheroids also influenced the process of tumor cells detaching from the tumor spheroid. In the experiment, spheroids of different sizes were generated and encapsulated in collagen matrices. With the increase of the diameter of the spheroids, the alignment coefficient and local density of collagen fibers became higher for a given distance of 180 μm between the tumor spheroids. Figure 4A displays the collagen density and fiber alignment coefficient in the region between the two tumor spheroids of different sizes. These results indicated that tumor spheroids remodeled the collagen fibers network by aggregating the fibers into a bundle-like network, which was positively correlated to their size.

As a consequence of matrix reorganization, the number of invading tumor cells and their polarity were highly dependent on the spheroid size (Fig. 4B and 4C). We can see that the larger the spheroids, the higher the number and the cell aspect ratio of invading tumor cells. As a result, the migration speed and directionality of tumor cells were increased with the growth of the tumor spheroids. Figure 4D shows a higher proportion of cells intending to invade along the center-center line between the two spheroids for larger spheroids.

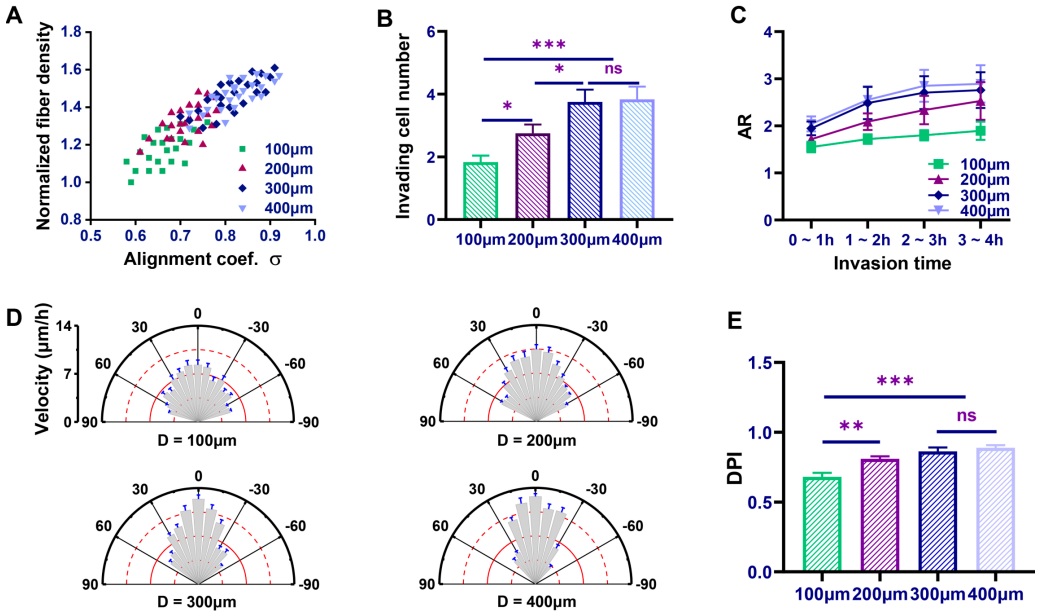

Fig. 4 Impact of tumor spheroid size on tumor cell invasion at a given spheroid distance of 180 μm. (A) Collagen density and fiber alignment coefficient of fiber matrix in the region between tumor spheroids for different spheroid sizes. (B) Number of invading tumor cells detached from the tumor spheroid per 100 μm arc length of the spheroids of various sizes. (C) The evolution of the aspect ratio of tumor cells as a function of invasion time for different spheroid sizes. (D) Sector distribution map of the mean velocity of invading tumor cells detached from the tumor spheroids of various sizes within 4 hours. (E) The DPI of the trajectory of invading tumor cells on tumor spheroids of different sizes within 4 hours. The statistical analysis of panels B and E was conducted using the one-way ANOVA method.

The elevation of the directionality of the trajectory of tumor cells with the size of tumor spheroids shown in Fig. 4E supported the results in Fig. 4D. However, the effect of spheroid size on the degree of collagen fiber remodeling and the invasion of tumor cells became saturated when it reaches a certain threshold. This threshold value depended on the spheroid distance. For instance, for the spheroid distance of 180 μm, the threshold diameter was approximately 300 μm. However, when the spheroid distance decreased to 120 μm, the effect of the spheroid size would then level off at the diameter of 200 μm (Fig. S5). Likewise, a similar size effect was observed for the invasion behaviors of single tumor spheroids (Fig. S6).

3.4 Effect of cell contraction on the invasion of dual-tumor spheroids

We have demonstrated that tumor cells could detach from one spheroid and invade towards the other via remodeling matrix fibers by generating active contraction force. At the same time, the contraction force produced significant tensile deformation in the collagen matrix. Therefore, it is interesting to ask about the role of the tension in tumor invasion. To investigate the effect of tension in tumor invasion, we regulated the active contraction of tumor spheroids by using Blebbistatin, an inhibitor of myosin-II-specific ATPase. The deformation in the matrix was substantially reduced by the inhibition of myosin activity with Blebbistatin (Fig. 5B and 5C), compared with that the fiber structure between the spheroids was notably deformed in control (Fig. 5A). The suppressive effect of Blebbistatin depended on the inhibitor concentration. When 2 μM blebbistatin was added to the culture media, the deformation of the fiber structure was slightly reduced (Fig. 5B). But with further addition of blebbistatin up to 10 μM, the fiber structure relaxed most of the deformation (Fig. 5C).

To better quantify the distortion of the fiber structure, ECM displacement was projected to the horizontal direction as a function of the distance from the right edge of the left spheroid. The results showed that the collagen fibers close to both left and right tumor spheroids underwent the most significant levels of displacement, with direction primarily towards the center of the tumor spheroid (Fig. 5D). In contrast, the fibers in the middle region experienced minimal displacement. When the contraction was inhibited, the deformation of the fiber matrix was significantly reduced. Correspondingly, inhibiting cell contraction led to a less ordered collagen fiber network, thereby hindering the invasion of tumor cells (Fig. 5E, F). Moreover, inhibition of contractile forces reduced tumor cell polarity (Fig. 5G), because cell polarization depended on both its active contraction and stiffness of fiber matrix.

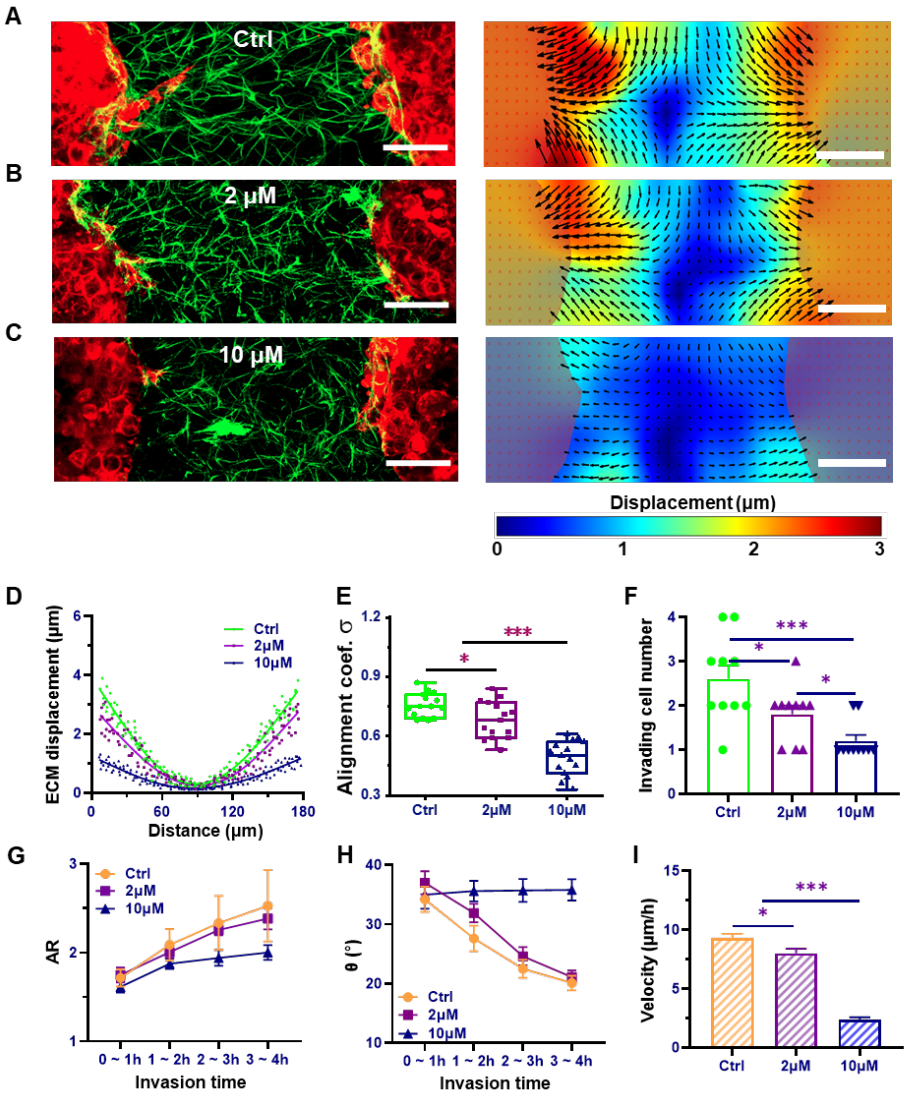

Fig. 5 Effect of cell active contraction on the invasion of tumor cells. (A-C) Fluorescence images of tumor invasion and the displacement field of ECM around 30 minutes after tumor spheroids were seeded in the matrix. (A) Control group without drug treatment; (B) Treatment with 2 μM blebbistatin for 4 hours; (C) Treatment with 10 μM blebbistatin for 4 hours. Red represents cells, and green represents collagen fibers. The scale bar is 50 μm. (D) Horizontal component of ECM displacement. Effect of the drug treatment compared with the control. (E) Alignment coefficient of collagen fibers in the region between the two tumor spheroids. Effect of the drug treatment compared with the control. (F) Number of invading tumor cells per 100 μm arc length of tumor spheroids with different drug treatments. (G) The aspect ratio of invading tumor cells as a function of invasion time for different drug treatments. (H) The angle θ as a function of invasion time for different drug treatments. (I) The mean velocity of invading tumor cells for different drug treatments. The statistical analysis of panels E, F, and I was conducted using the one-way ANOVA method.

We further explored the influence of cellular contractility on the direction of tumor cell invasion. Low dose of Blebbistatin had slight effects on the direction of cell migration/polarization (Fig. 5H), as it showed moderate influence on the ability of tumor spheroids to remodel the collagen fibers. High level of inhibition substantially increased the angle θ compared to control and low dose treatment, and thus, the direction of tumor cell invasion became more random (Fig. 5H). Moreover, inhibiting cell contraction significantly reduced the velocity of tumor cell invasion (Fig. 5I), as inhibition not only reduced the ability of cells to remodel the collagen fiber matrix, but also eliminated the driving force of cell migration. Similar results were observed when the distance of the two tumor spheroids was changed to 120 μm and in the single tumor spheroid system (Fig. S7 and Fig. S8). Interestingly, for single-tumor spheroids, treatment with 2 μM blebbistatin increased the velocity of cell invasion (Fig. S8F), while having no significant effects on the alignment coefficient of fibers, the number and polarization of invading cells (Fig. S8A-E). These findings suggest that tumor cell invasion may be initiated by contractility-induced matrix remodeling.

3.5 Tension release in collagen fibers impedes tumor invasion

We have just shown that cell active contraction played significant roles in the remodeling of the fibers matrix through inhibiting cytoskeleton contractility. However, the inhibition may at the same time influence the structural integrity of cells themselves. Therefore, to eliminate this effect, we decided to release the tension in the matrix by using a purely mechanical approach. To this end, we employed the pulsed laser with a wavelength of 800 nm to ablate the fiber matrix close to the tumor-spheroids. We performed photoablation at two different locations, which were l =60 and 80 μm away from the edge of the tumor-spheroids (Fig. 6A &B). Presumably, matrix photoablation near the spheroid can disrupt large amount of matrix tension.

We found that the number of invading cells near the ablated region was lower than that of other regions (Fig. 6A-C). Notably, the effects on tumor cell invasion were more obvious when

the ablation distance was 60 μm compared to 80 μm, supported by the considerable reduction in both the number of invading cells and their invasion displacement in the ablation region/direction (Fig. 6C and 6D).

To further confirm the effects of tension release on tumor invasion, we examined the tumor protrusion formation process in the vicinity of laser ablation in response to the tension reduction. We found that there was a prominent retraction of cell protrusion after ablation at 60 μm instead of 80 μm compared to the results of no ablation control (Fig. 6E-H). These results suggested that ablation impeded tumor cell protrusion by releasing the tension in the cell-matrix system. Therefore, these results suggested that the tension forces in the fiber matrix played a vital role in tumor invasion, and release of the tension prohibited the invasion.

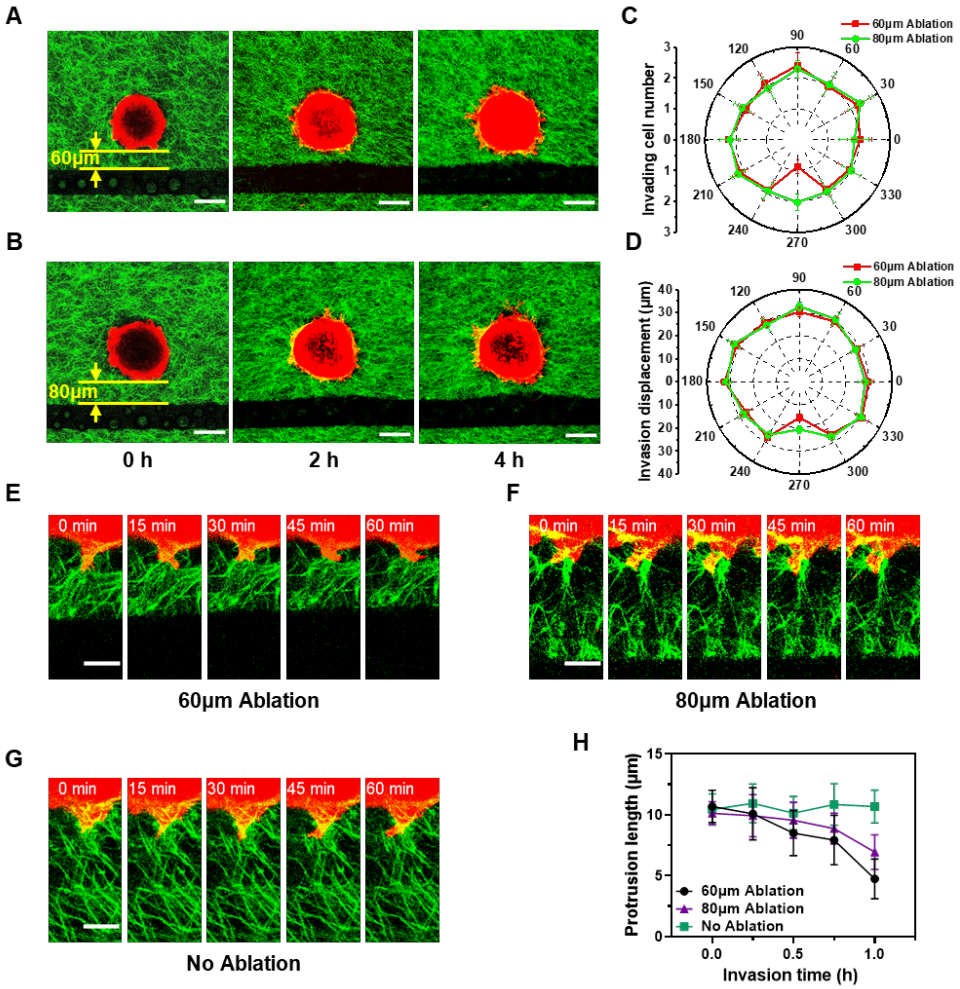

Fig. 6 Effect of tension release by laser ablation in matrix on tumor invasion. (A) and (B) Fluorescence

images of single tumor invasion after laser ablation at l =60 and 80 μm, respectively, for three time points (0, 2, and 4 hours after the ablation). Red is the cell, and green is the collagen fiber. Scale bar, 100 μm. (C) Polar graph plotting the line graph of the circumferential distribution of invading cell number on the edge of tumor spheroid at 4 h. (D) Polar graph plotting the line graph of circumferential distribution of invasion displacement on the edge of tumor spheroid at 4 h. (E-F) Time-lapse fluorescence images of the evolution of protrusion at varied time after ablation at l =60 or 80 μm compared with control (G). Scale bar, 25 μm. (H) The length of cell protrusion as function of time after ablation at l =60 or 80 μm compared with control.

3.6 Numerical simulation of tumor invasion behaviors

3.6.1 Effect of physical factors on the invasion process

To understand the underlying mechanisms of tumor invasion, numerical models were adopted to simulate the invasion process (Fig. S1). The effects of spheroid distance, fiber density, spheroid size, cell contraction, and basement membrane stiffness were analyzed. In the simulation, the cells of the left spheroid were allowed to migrate and invade.

Figure 7A-F show the snapshots of the final state of tumor cell invasion (in red) over a given time period under various conditions. We can see that there was a significant structural evolution of the tumor spheroids and remodeling of the fiber matrix under the contraction of tumor cells. The fibers were pulled along the line connecting the two spheroids to facilitate the invasion of tumor cells into the matrix in the region between the cell spheroids. The simulations showed that increasing the spheroid distance, the fiber density, or decreasing cell contraction reduced the number of invading cells (Fig. 7B, C, E, G). However, increasing the size of the tumor spheroid promoted the cells to detach and invade (Fig. 7D).

We also considered a cortex membrane structure around the tumor spheroid in our model to simulate the basement membrane of tumor tissue. Clearly, increasing the stiffness of the basement membrane significantly suppressed the detachment of tumor cells (Fig. 7F and 7G).

In addition, we calculated the time required for the first tumor cells to detach from the tumor spheroid, referred to as the time required for cell detachment (Fig. 7H). The results showed that large separation distance between the two spheroids, high fiber density, small

contraction, and stiff basement membrane retarded tumor cell invasion, while large tumor spheroids facilitated this process.

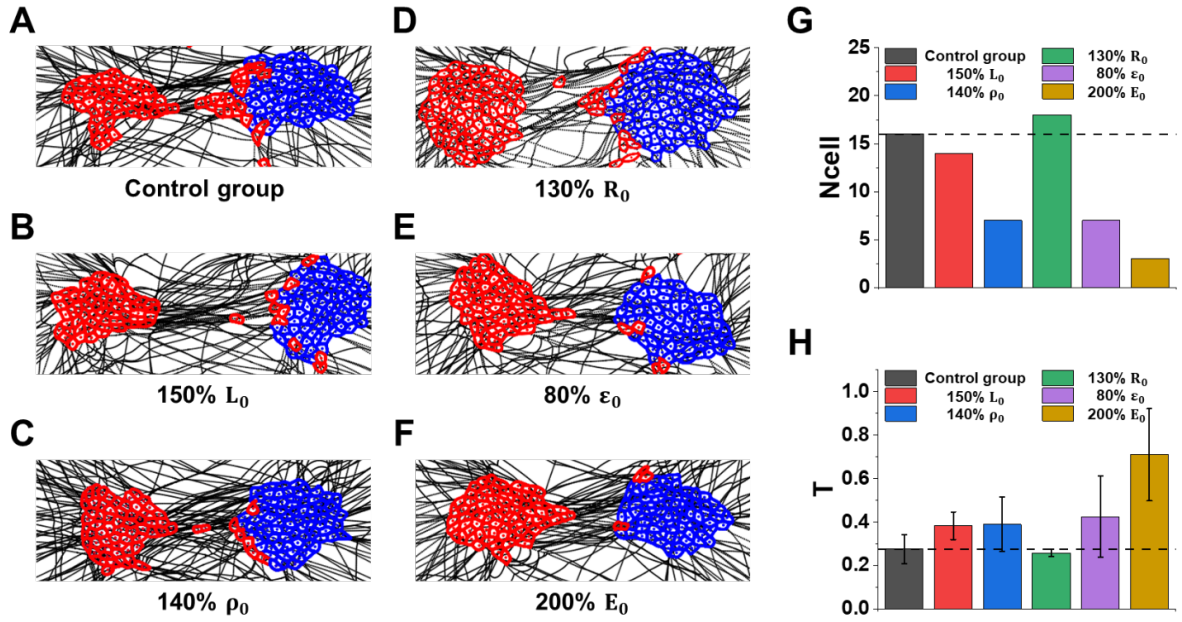

Fig. 7 Numerical simulations of the effect of various physical factors on tumor cell invasion. (A) Control group; (B) Larger spheroid distance (150% L_0); (C) Higher fiber density (140% ρ_0); (D) Larger tumor spheroid size (130% R_0); (E) Smaller cell contraction (80% ε_0); (F) Higher stiffness of basement membrane (200% E_0); Cells of the left tumor spheroid are shown in red, while those of the right tumor are in blue. (G) Statistical data on the number of tumor cells that detached from the spheroids. (H) Statistical data on the average time for tumor cells detaching from the spheroids.

Our numerical simulation recapitulated the experimental findings, demonstrating how various physical factors influenced the invasion process. This achievement can be attributed to our model' ability to not only describe complex mechanical interactions, such as cell-cell interactions and cells-matrix fiber interactions, but also incorporate the effect of supercellular structure in tumor tissue that had not been considered in previous studies.

3.6.2 Deformation and alignment of matrix fiber and their effect on cell invasion

To understand the underlying mechanisms of the effect of different factors on the invasion of tumor cells, we simulated the dynamic remodeling process of the fiber network and associated tumor invasive process under various conditions. We obtained the strain field in the fiber matrix (Fig. 8A-F), of which the mean strain of the fibers was summarized in Fig. 8G. We can see that there were larger fiber strains in the region between the tumor spheroids than the other region. Increasing the stiffness of the basement membrane or the size of tumor spheroids led to higher fiber strain, whereas increasing the spheroids distance and fiber density and reducing the cell active contraction resulted in lower fiber strain.

We further analyzed the fiber alignment of the remodeled matrix (Fig. 8H). We can see that the contraction of tumor spheroids led to a more ordered fiber alignment. Considering the results in Fig. 8G, we showed that the larger fiber strain was associated with a more ordered fiber alignment. These results suggested the correlation between the deformation and alignment of fibers and might further supported the effects of these factors on tumor invasion (Fig. 7). For instance, there is a positive correlation between the velocity of detached tumor cells and the degree of fiber alignment (Fig. 8I), recapitulating our experimental results (Fig. 2). And the ordered fiber network facilitated the persistence of cell migration (Fig. 8J). The more ordered the fiber alignment, the less likely the cells altered their direction, leading to persistent migration from one spheroid to the other.

Together, these simulation results demonstrated the close relation between the invasive ability of tumor cells and the mechanical properties of the local microenvironment, specifically the fiber strain and alignment, which impacts not only the detachment of tumor cells but also their migration velocity and persistence. These results were consistent with the experimental results of number of invasive cells and fiber alignment (Fig. 2E &G).

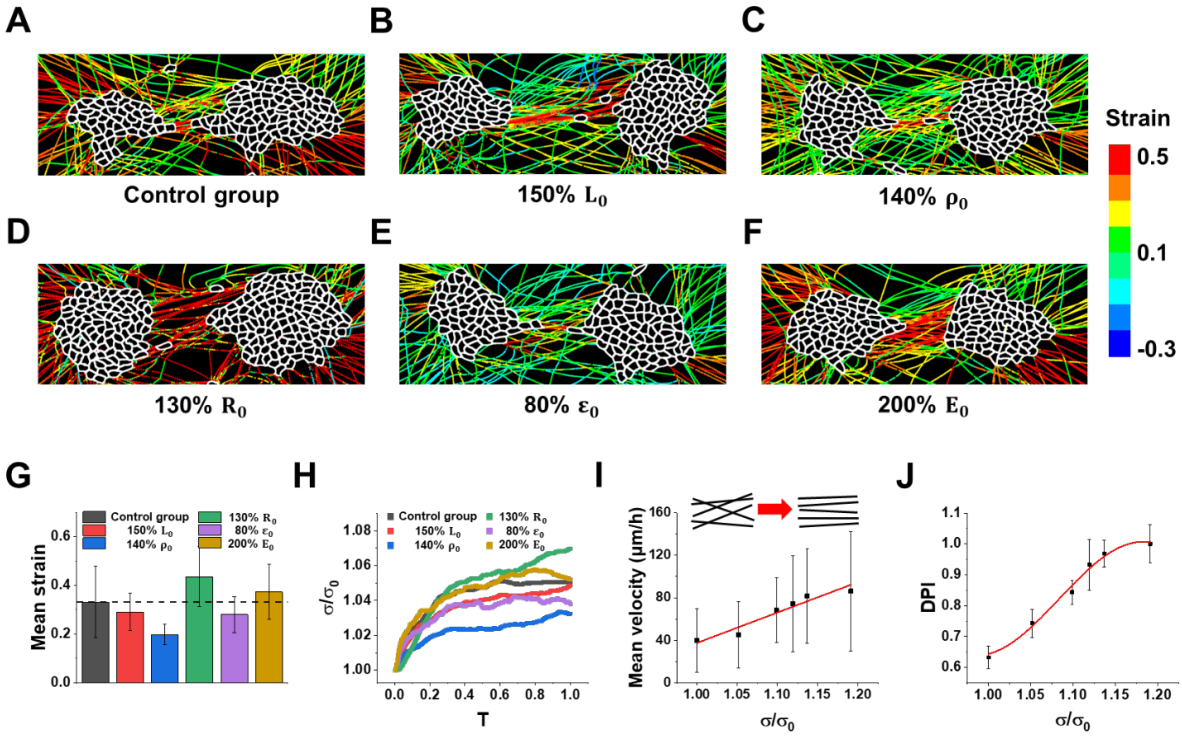

Fig. 8 Effect of fiber strain and alignment on tumor cell invasion under various conditions. (A-F) Simulation results of ECM fiber strain due to the remodeling of fiber matrix by tumor spheroids: (A) Control group; (B) Larger spheroid distance (150% L_0); (C) Higher fiber density (140% ρ_0); (D) Larger tumor spheroid size (130% R_0); (E) Lower cell contraction (80% ε_0); (F) Higher stiffness of base membrane (200% E_0). (G) Statistical results of the mean strain of fibers in the region between the two tumor spheroids. (H) Normalized alignment coefficient of fibers as a function of normalized time. (I) Relationship between the mean velocity of detached tumor cells and the normalized fiber alignment coefficient. (J) Relationship between the DPI of detached tumor cells and the normalized fiber alignment coefficient.

3.6.3 ECM fibers modulate the polarization of detached tumor cells

We further examined the distribution/variation of the aspect ratio of tumor cells under various conditions (Figs. 9A-F), revealing that the detached tumor cells typically exhibited a higher aspect ratio than the undetached cells within the tumor spheroid. Moreover, cells in the periphery of the spheroid displayed a higher aspect ratio than those in the interior region, possibly owing to the effect of the stress-induced cell polarization.[34, 35]

We found that cell aspect ratio plays important roles in the cell detaching and invasion process. For instance, there is a linear relationship between the persistence of cell migration and cell

polarization (Fig. 9G). Since the aspect ratio of cells was closely related to migration ability, the higher the cell aspect ratio, the higher the persistence of cell migration. Figure 9H illustrates a positive correlation between cell aspect ratio and the number of detached tumor cells, suggesting cell detachment from the spheroid was closely related to the cell polarization. This simulation result was consistent with our experimental results shown in Fig. 2G & 2I. We found that the cell aspect ratio increased nonlinearly with the fiber strain, and eventually leveled off to a constant value (Fig. 9I). This phenomenon is consistent with the matrix-stiffness dependent polarization of cells on 2D matrix.

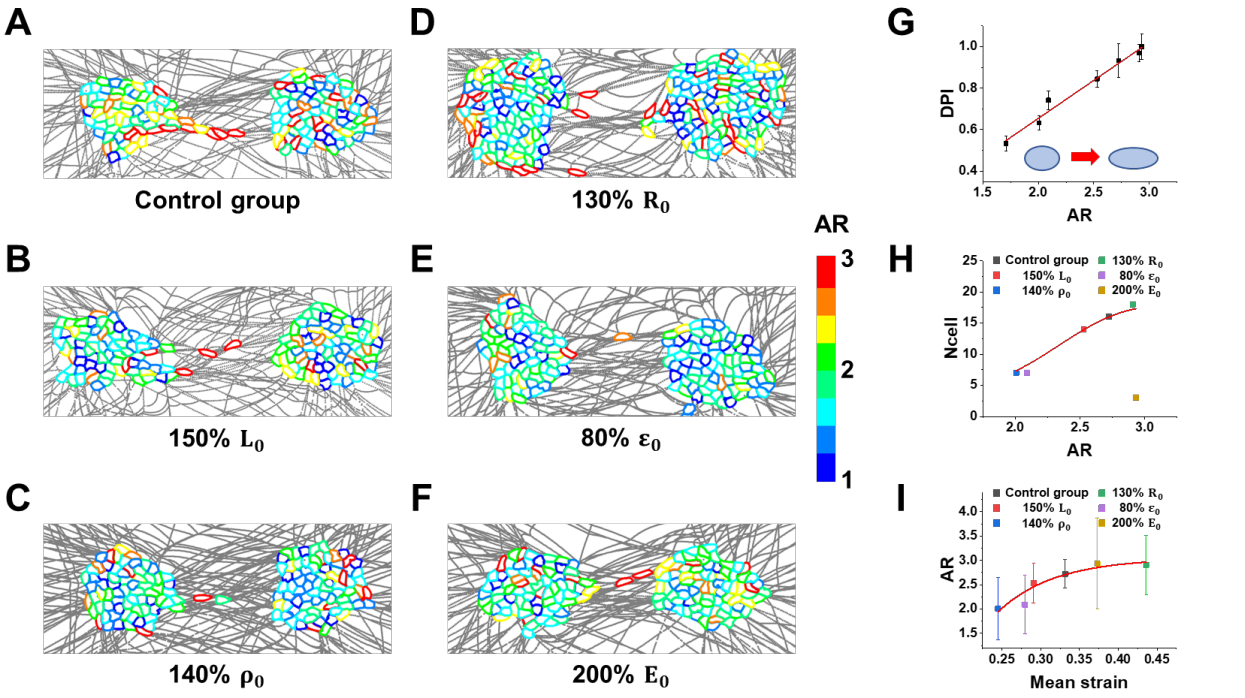

Fig. 9 The distribution and variation of polarity (aspect ratio) of tumor cells. (A-F) The color maps depict the simulation results of cell aspect ratio under various conditions: (A) Control group; (B) Larger spheroids distance (150% L_0); (C) Higher fiber density (140% ρ_0); (D) Larger tumor spheroids size (130% R_0); (E) Smaller cell contraction (80% ε_0); (F) Higher stiffness of the base membrane (200% E_0). (G) Relationship between the persistent of cell migration and cell polarity. (H) Relationship between the number of detached tumor cells and their polarity. (I) Relationship between the polarity of detached tumor cells and fiber strain.

4. Discussion and conclusions

4.1 Tensional force by cell contraction plays key roles in tumor invasion

It has been realized that cell and tissue's active contraction developed a tensional force field around them, which could be finely regulated by cell and tissue in a somehow balanced and consistent manner, called tensional homeostasis.[34, 36, 37] Tensional homeostasis was thought to be the hallmark of the living systems.[37] And the tumor tissue is no exception. In this study, we showed that the tension caused by the active contraction of cells and tumor play important roles in two aspects of the tumor invasion behaviors. One is to remodel the matrix, and the other one is to polarize the cell and regulate the cell-matrix interaction.

We showed that there were significant structural changes in the tumor spheroid and fiber matrix under the tensional stress developed by the contraction of tumor tissue. The fibers were pulled and re-organized along the line connecting the two spheroids. The alignment coefficient of collagen fibers surrounding tumor spheroids gradually increased over time. When the fibers were remodeled to certain level, the tumor cells invaded along the fibers into the matrix in the region between the two spheroids. In addition, we showed that the degree of remodeling was non-uniform, and there was a higher fiber density and a higher degree of alignment near the invasive sites compared to non-invasive sites (Fig. S2E).

In addition to the structural change, the tensional force also caused significant deformation in the fibers, which caused stiffening of the fibers as they are hyperelastic materials, i.e., fiber stiffness increases with the deformation. The fibers' stiffening would further enhance the cell-fiber interaction, and then promote cell polarization and invasive migration. According to the traction-distance law,[34, 35] cells with a larger aspect ratio could generate a higher driving force for migration by regulating the adhesion at the cell front and the deadhesion at the cell rear.[31, 32] Previous experiments confirmed that tensile loading could promote cell polarization and migration.[38] Our results showed that there was higher tension at the boundary of the tumor spheroid because of the active contraction by tumor cells and tissue.[34, 39] These results may

explain why the cells at the edge of the tumor had a large aspect ratio and were more likely to detach from tumor tissue.

These results suggested that the tensional force field was crucial for the remodeling of the matrix and invasive migration of tumor cells. Our results showed that tumor invasion was typically accompanied by continuous remodeling of the ECM fiber network. Since tumor cells needed to form focal adhesion with the ECM fibers for migration, the more orderly the fibers remodeled by tumor spheroids, the greater the probability of tumor cells migrating along the direction of the central line between the spheroids. We also discovered that better fiber alignment led to increased cell migration persistence (Fig. 2). It can be anticipated that when tumor cells migrated along the finely aligned fibers, they would encounter fewer branching pathways, leading to higher migration persistence and velocity.[29]

We confirmed these findings by relaxing the tensional stress using an inhibitor or laser ablation. Our results revealed that blebbistatin inhibitor significantly reduced the tumor invasion (Figs. 5A-C). Blebbistatin weakened myosin activity and thus reduced the deformation and stiffness of the fiber matrix. In addition, blebbistatin treatment could reduce the stability of focal adhesions.[40] Our results showed that the treatment with blebbistatin significantly weakened the degree of fiber remodeling (Fig. 5E), ultimately resulting in a decrease in cell invasion ability (Fig. 5I). On the other hand, when the fiber matrix was ablated by laser beam, the tension in the fiber matrix near the ablation was significantly relaxed, causing the retraction of cell lamellapodium, which equivalently impeded the invasion of tumor cells.

Our results further showed that there was an intensive mechano-chemical coupling in cell and tissue behaviors. Cell polarization and alignment were driven by the stress field in the tissue,[34, 35] which is called the stress-driven cell behaviors. The active contraction of cells and tissue could regulate the stress field in the tissue and the remodeling of the fibril ECM. Since stress distribution was non-uniform in the tissue, so was the degree of cell polarization. Coincidentally, the polarization of cells at the edge of the tumor spheroid was comparatively high, which was

crucial for their detaching from the tumor.

4.2 Physical factors that influence the tensional field and cell invasion

It is known that there are various mechanical cues in the tumor microenvironment that can regulate cancer development, including matrix stiffness,[41, 42] microstructure,[26, 43] and geometric confinement.[44] This study demonstrated that these physical factors could impact the tumor invasion process by regulating the tensional force field in the tumor-matrix system.

We found that by increasing the distance between tumor spheroids, the degree of fiber alignment was significantly reduced. Our numerical simulation revealed that with the increase of the spheroid distance it became more difficult to develop higher tensional force within an enlarged volume of fiber matrix, which resulted in small tension force and less degree of remodeling of fiber matrix. On the other hand, decreasing cell active contraction by inhibitor or laser ablation would also reduce the tension force in the fiber matrix. Therefore, both approaches result in a significant decrease in the fiber strain and the degree of fiber alignment. In contrast, increasing tumor spheroids led to increased fiber strain and structural realignment.

Interestingly, fiber density plays a biphasic effect on tumor invasion, suggesting that fiber density had multifaceted effects on cell-matrix interaction. It would affect both matrix stiffness and the remodeled structure of the fiber matrix. For instance, for low fiber density, although compliant fiber structures facilitate the remodeling of the matrix, an insufficient quantity of fibers cannot provide adequate support for cell adhesion and migration.[45] Conversely, when the matrix stiffness is increased to the point where the contractile force generated by tumor cells can not effectively remodel the fibers (despite high stiffness being beneficial for cell adhesion), the result is a lower degree of fiber alignment, which then becomes unfavorable for cell invasion. Therefore, there is a balanced fiber density for efficient tumor invasion (Figs. 6E, G). Our numerical simulation captured this biphasic dependence of the tumor invasion on the fiber density (Fig. S9 in the Supplementary Materials).

In summary, our research indicated that in the complex process of tumor invasion, the active

contraction force of the tumors produced a tensional force field in the tumor-fiber matrix system, which not only remodeled the fiber matrix, but also guided the polarization of tumor cells, which ultimately determined the invasion behaviors of tumor cells. Our numerical simulation quantitatively analyzed the tensional force field, and displayed that how the tensional force field influence the polarization of the tumor cell during the cell invasion process. These numerical results revealed a mechano-chemical coupling mechanism in tumor invasion, i.e., how the tensional field coupled with the polarization of tumor cells, which revealed the underlying cellular mechanisms of regulation of the tumor invasion processes.

Acknowledgement

This work was supported by funds from the National Natural Science Foundation of China (Grant Nos. 11932017, 12122212, and 11972316), Shenzhen Science and Technology Innovation Commission (Project no. JCYJ20200109142001798 and JCYJ20220531091002006), and Health and Medical Research Fund (HMRF18191421).

Competing interests

All authors of this paper declare no conflict of interest in this work.

References

1. S. Valastyan and R. A. Weinberg, *Cell*, 2011, **147**, 275-292.
2. A. W. Lambert, D. R. Pattabiraman and R. A. Weinberg, *Cell*, 2017, **168**, 670-691.
3. Y. Yuan, Y.-C. Jiang, C.-K. Sun and Q.-M. Chen, *Oncol. Rep.*, 2016, **35**, 2499-2515.
4. C. T. Mierke, *Rep. Prog. Phys.*, 2019, **82**, 064602.
5. D. T. Butcher, T. Alliston and V. M. Weaver, *Nat. Rev. Cancer.*, 2009, **9**, 108-122.
6. P. Lu, V. M. Weaver and Z. Werb, *J. Cell Biol.*, 2012, **196**, 395-406.
7. T. R. Cox and J. T. Erler, *Dis. Model. Mech.*, 2011, **4**, 165-178.
8. P. Schedin and P. J. Keely, *Cold Spring Harb. Perspect. Biol.*, 2011, **3**, a003228.
9. J. S. Bredfeldt, Y. Liu, M. W. Conklin, P. J. Keely, T. R. Mackie and K. W. Eliceiri, *J.*

Pathol. Inform., 2014, **5**, 28.
10. M. W. Conklin, J. C. Eickhoff, K. M. Riching, C. A. Pehlke, K. W. Eliceiri, P. P. Provenzano, A. Friedl and P. J. Keely, *The American journal of pathology*, 2011, **178**, 1221-1232.
11. M. Fang, J. Yuan, C. Peng and Y. Li, *Tumor Biol.*, 2014, **35**, 2871-2882.
12. A. Nagelkerke, J. Bussink, A. E. Rowan and P. N. Span, *Semin. Cancer Biol.*, 2015, **35**, 62-70.
13. G. Huang, L. Wang, S. Wang, Y. Han, J. Wu, Q. Zhang, F. Xu and T. J. Lu, *Biofabrication*, 2012, **4**, 042001.
14. L. Feller, R. A. G. Khammissa and J. Lemmer, *Cancer Cell Int.*, 2017, **17**, 1-6.
15. S. Löffek, C.-W. Franzke and I. Helfrich, *Int. J. Mol. Sci.*, 2016, **17**, 1910.
16. L. Chin, Y. Xia, D. E. Discher and P. A. Janmey, *Current opinion in chemical engineering*, 2016, **11**, 77-84.
17. A. Chronopoulos, B. Robinson, M. Sarper, E. Cortes, V. Auernheimer, D. Lachowski, S. Attwood, R. García, S. Ghassemi and B. Fabry, *Nat. Commun.*, 2016, **7**, 12630.
18. Y. L. Han, A. F. Pegoraro, H. Li, K. Li, Y. Yuan, G. Xu, Z. Gu, J. Sun, Y. Hao and S. K. Gupta, *Nat Phys*, 2020, **16**, 101-108.
19. T. Koorman, K. A. Jansen, A. Khalil, P. D. Haughton, D. Visser, M. A. Rätze, W. E. Haakma, G. Sakalauskaitè, P. J. van Diest and J. de Rooij, *Oncogene*, 2022, **41**, 2458-2469.
20. W. Han, S. Chen, W. Yuan, Q. Fan, J. Tian, X. Wang, L. Chen, X. Zhang, W. Wei and R. Liu, *Proc. Natl. Acad. Sci.*, 2016, **113**, 11208-11213.
21. H. Ahmadzadeh, M. R. Webster, R. Behera, A. M. Jimenez Valencia, D. Wirtz, A. T. Weeraratna and V. B. Shenoy, *Proc. Natl. Acad. Sci.*, 2017, **114**, E1617-E1626.
22. A. Pal, P. Haliti, B. Dharmadhikari, W. Qi and P. Patra, *IEEE/ACM Trans. Comput. Biol. Bioinform.*, 2020, **18**, 2566-2576.
23. Y. Li, H. Naveed, J. Liang and L. X. Xu, 2014.
24. E. B. Berens, J. M. Holy, A. T. Riegel and A. Wellstein, *JoVE (Journal of Visualized Experiments)*, 2015, DOI: 10.3791/53409, e53409.
25. J. Y. Tee and A. Mackay-Sim, *Int. J. Mol. Sci.*, 2021, **22**, 9177.
26. K. M. Riching, B. L. Cox, M. R. Salick, C. Pehlke, A. S. Riching, S. M. Ponik, B. R. Bass, W. C. Crone, Y. Jiang and A. M. Weaver, *Biophys. J.*, 2014, **107**, 2546-2558.
27. I. C. Valadão, A. C. L. Ralph, F. Bordeleau, L. M. Dzik, K. S. Borbely, M. V. Geraldo, C. A. Reinhart-King and V. M. Freitas, *PeerJ*, 2020, **8**, e9153.
28. J. K. Sveen, *Journal*, 2004.
29. X. Xu, J. Xu, X. Li, J. Song, D. Li and B. Ji, *J Appl Mech*, 2022, **89**, 051005.
30. J. Y. Xu, X. Y. Xu, X. J. Li, S. J. He, D. C. Li and B. H. Ji, *Biophys. J.*, 2022, **121**, 288-299.
31. Y. Zhong and B. Ji, *Biofabrication*, 2013, **5**, 015011.

32. Y. Zhong and B. Ji, *Eur Phys J Spec Top*, 2014, **223**, 1373-1390.
33. F. Wei, X. Xu, C. Zhang, Y. Liao, B. Ji and N. Wang, *Nat. Commun.*, 2020, **11**, 4902.
34. S. He, Y. Green, N. Saeidi, X. Li, J. J. Fredberg, B. Ji and L. M. Pismen, *J Mech Phys Solids*, 2020, **137**, 103860.
35. S. He, Y. Su, B. Ji and H. Gao, *J Mech Phys Solids*, 2014, **70**, 116-135.
36. S. He, X. Li and B. Ji, *Acta Mech Sinica*, 2019, **35**, 275-288.
37. B. Ji, Mechanobiology and Mechanomedicine: tuning the tension in the life, https://imechanica.org/node/25467).
38. C. Li, F. Wernig, M. Leitges, Y. Hu and Q. Xu, *The FASEB journal*, 2003, **17**, 1-21.
39. S. He, C. Liu, X. Li, S. Ma, B. Huo and B. Ji, *Biophys. J.*, 2015, **109**, 489-500.
40. M. S. Shutova, A. Y. Alexandrova and J. M. Vasiliev, *Cell Motil. Cytoskeleton*, 2008, **65**, 734-746.
41. O. Chaudhuri, S. T. Koshy, C. Branco da Cunha, J.-W. Shin, C. S. Verbeke, K. H. Allison and D. J. Mooney, *Nat. Mater*, 2014, **13**, 970-978.
42. N. L. Habbit, B. Anbiah, L. Anderson, J. Suresh, I. Hassani, M. Eggert, A. Brannen, J. Davis, Y. Tian and B. Prabhakarpandian, *Acta Biomater.*, 2022, **147**, 73-90.
43. E. N. Horst, C. M. Novak, K. Burkhard, C. S. Snyder, R. Verma, D. E. Crochran, I. A. Geza, W. Fermanich, P. Mehta and D. C. Schlautman, *Acta Biomater.*, 2022, **146**, 222-234.
44. K. Alessandri, B. R. Sarangi, V. V. Gurchenkov, B. Sinha, T. R. Kießling, L. Fetler, F. Rico, S. Scheuring, C. Lamaze and A. Simon, *Proc. Natl. Acad. Sci.*, 2013, **110**, 14843-14848.
45. K. M. Yamada and M. Sixt, *Nat. Rev. Mol. Cell Biol.*, 2019, **20**, 738-752.